THE ASTROPHYSICAL JOURNAL, 273:24–35, 1983 October 1

REDSHIFTS OF GROUPS AND CLUSTERS IN THE RICH SUPERCLUSTERS 1451+22 AND 1615+43

ROBIN CIARDULLO
University of California, Los Angeles

HOLLAND FORD
University of California, Los Angeles; and Space Telescope Science Institute

FRANK BARTKO
Martin Marietta Corporation, Denver

AND

RICHARD HARMS
University of California, San Diego
Received 1982 December 28; accepted 1983 March 21

ABSTRACT

Redshift measurements and finding charts are presented for galaxy clusters in the field of two rich, distant superclusters. Both systems are shown to have morphological and dynamical properties similar to the nearby superclusters, including small internal velocity dispersions and high density contrasts in redshift space. This data is consistent with two interpretations: Either both superclusters are highly flattened systems with major axes close to the plane of the sky, or the observed velocity dispersions do not arise from unperturbed Hubble flow. If the latter explanation is correct, these radial velocity data are a powerful probe of the large scale matter density in the universe.

Subject headings: galaxies: clustering — galaxies: redshifts

I. INTRODUCTION

Superclusters are the largest aggregates of matter in the universe. Statistical studies, such as those by Abell (1961), Bogart and Wagoner (1973), and Hauser and Peebles (1973), have shown that superclusters have transverse dimensions of $\sim 50h^{-1}$ Mpc ($h = H_0/100$) and typically consist of two or three rich clusters, although some very rich superclusters may be comprised of 10 or more clusters (Abell 1961; Murray *et al.* 1978). Although these studies established the existence of superclusters and inferred some of their statistical properties, they did not provide insight into the dynamical structure or evolutionary state of superclusters.

Rood (1976) made an important departure from the statistical studies when he used the redshifts of all distance class 3 or nearer Abell clusters to investigate the three-dimensional distribution of nearby rich clusters. Rood confirmed the previous findings and estimated that 40% of all rich clusters are in high density contrast superclusters. He also analyzed the ratio of the mean transverse velocities to the mean radial velocity differences and concluded that superclusters are part of an unperturbed Hubble flow. Thuan (1980) reached similar conclusions from an analysis of a larger redshift sample which comprised a complete sample of Abell clusters with distance classes less than or equal to 4.

Four nearby superclusters have been thoroughly studied by measuring the radial velocities of all galaxies to a specified limiting magnitude: the Local Supercluster (cf. de Vaucouleurs 1975*a*, *b*; Tully 1982), Coma/A1367 (Gregory and Thompson 1978), Hercules/A2197 (Tarenghi *et al.* 1979, 1980; Chincarini, Rood, and Thompson 1981), and Perseus (Gregory, Thompson, and Tifft 1981). These studies have shown that nearby superclusters have characteristic sizes of $\sim 50h^{-1}$ Mpc, high redshift-space density contrast relative to their surroundings, and apparently flattened and filamentary shapes.

This paper presents the data from a redshift survey of clusters in two rich, distant superclusters, 1451+22 (=Abell 11 [Abell 1961] = MFJG 18 [Murray *et al.* 1978]) and 1615+43 (=MFJG 19). Preliminary results and analysis of the data have been presented in previous papers (Ford *et al.* 1981, hereafter Paper I; Harms *et al.* 1981, hereafter Paper II). A more complete analysis of the data will be presented in a subsequent paper.

II. OBSERVATIONS AND REDUCTION

The data were collected with the Lick Image Tube Scanner (ITS; Robinson and Wampler 1972; Miller, Robinson, and Wampler 1976; Miller, Robinson, and Schmidt 1980) at the Cassegrain focus of the Shane 3 m telescope. For all of the objects, except those observed in 1981 April, the "red" image tube chain was used. This detector has an S-25 photocathode and a high sensitivity at 6000 Å. The 1981 April observations were made with the "green" image tube chain, which has its peak sensitivity at 4000 Å. The grating used has 600 l mm^{-1} and is blazed at 5000 Å in first order. The grating-detector combination yields a resolution of

~11 Å (FWHM) and gives 2500 Å of spectral coverage. Nearly all of our spectra were centered at 5150 Å.

Our program consisted of taking spectra of galaxies in the rich Abell clusters (Abell 1958) projected in and around the superclusters 1451+22 and 1615+43. Typically, we observed the three brightest galaxies projected near the center of each cluster. These galaxies have the highest *a priori* probability of being cluster members and, by virtue of having formed or settled near the bottom of the cluster's potential well, have the least dispersion about the cluster's mean velocity.

In addition to observing rich clusters, we searched the Palomar Observatory Sky Survey prints for poor clusters and groups which could also serve as test particles in the superclusters' gravitational fields. We selected and observed candidate galaxies which are comparable in brightness and color to the brightest rich cluster galaxies and are within 6° of the nominal supercluster centers. In all, our sample, collected over a 3 yr period, consists of 75 galaxies in 44 clusters in the area of 1451+22, and 49 galaxies in 24 clusters in and around 1615+43.

The observations were reduced with the UCLA Fortran Scanner Data Reduction System (FSDRS; Grandi 1982). Pixel-to-pixel irregularities in the image-tube response were removed by dividing the data by the spectrum of a continuum lamp taken at the beginning and ending of each night. Wavelengths were determined from fifth-order polynomial least square fits of comparison spectra obtained at or near the telescope position of each object. The rms residuals of these fits were typically ~35 km s^{-1}. Absolute fluxes were calculated using the standard stars calibrated by Stone (1977).

With the exception of four foreground galaxies, all of the galaxies displayed the characteristic early type galaxy spectrum reproduced in Figure 1. Redshifts were determined as follows:

Each spectrum was reduced to F_λ and plotted versus the logarithm of wavelength. The logarithmic scale removes the wavelength-dependent redshift stretching and thus allows galaxies with different redshifts to be easily registered against one another. Using this technique, the spectral lines and continuum slope of each program galaxy were visually correlated with a high signal-to-noise ratio template galaxy to yield a relative redshift.

A set of absolute redshifts for each galaxy was then found by measuring the wavelengths of calcium K and H (λ3933.6, 3968.5), the G band (λ4303.4), and the Mg I *b* band (λ5175.4). Small correction factors, derived from the redshift measurements of the airglow and San Jose cityglow lines, were applied to these redshifts, to compensate for the effects of instrument flexure and systematic deviations in the wavelength calibration. These corrected absolute redshifts were averaged with the relative redshift to yield the adopted redshift value appearing in the fifth column of Table 1. Typically, these redshifts have internal errors of ~100 km s^{-1}.

The quality and confidence of our redshift measurements are also listed in Table 1. The quality index "A" indicates a high signal-to-noise spectrum with a small internal measurement error. A "B" quality still represents a well-determined redshift but reflects a lower signal-to-noise spectrum with one or more of the spectral lines poorly defined. Quality "C" redshifts are based only on the possible identification of one or two spectral features and are uncertain. Figure 1 illustrates this classification.

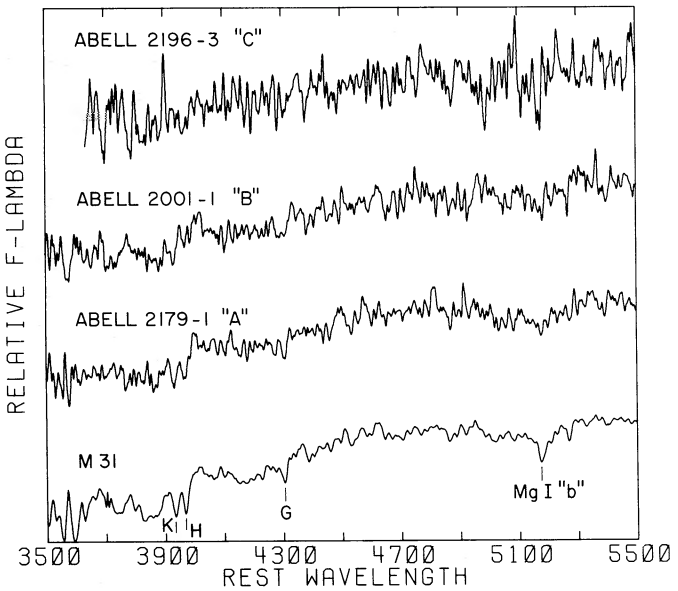

FIG. 1.—The spectra of three observed galaxies with redshift confidences A, B, and C, plotted in their rest frame. Displayed below them is the spectrum of the bulge of M31. Note the characteristic continuum shape, common to all early-type galaxies.

TABLE 1

OBSERVATIONAL DATA ON SUPERCLUSTERS 1451+22 AND 1615+43

SUPERCLUSTER 1451+22 GALAXIES

CLUSTER	DATE	α(1950)	δ(1950)	z	Q	Notes
ABELL 1960-1	6-13-80	14 42 13.49	19 34 05.2	0.1876	B	
ABELL 1972-1	4-16-80	14 46 17.62	24 11 17.0	0.1189	A-	S
ABELL 1976-1	6-06-78	14 48 01.77	21 08 35.9	0.1159	A	S
ABELL 1976-2	6-06-78	14 48 01.04	21 08 32.8	0.1175	A	S
ABELL 1976-3	6-06-78	14 48 06.30	21 08 09.3	0.1176	A-	S
ABELL 1980-1	6-05-78	14 49 15.51	22 50 13.0	0.1156	B-	S
ABELL 1980-2	6-05-78	14 49 14.73	22 50 54.2	0.1139	B	S
ABELL 1980-3	6-23-79	14 49 17.49	22 51 04.7	0.1144	C+	S
ABELL 1984-1	2-06-81	14 50 23.86	28 10 16.2	0.1242	B	
ABELL 1986-1	6-03-78	14 50 54.18	22 06 18.1	0.1170	A	S
ABELL 1986-2	6-03-78	14 50 47.24	22 07 35.7	0.1170	B-	S
ABELL 1986-3	6-04-78	14 50 43.15	22 06 12.1	0.1218	B+	S
ABELL 1988-1	5-27-79	14 51 26.88	20 56 46.0	0.1157	B-	S
ABELL 1988-2	5-27-79	14 51 23.23	20 56 08.6	0.1150	B	S
ABELL 1988-3	5-27-79	14 50 58.39	21 01 56.0	0.1187	C+	S
ABELL 1988-4	6-22-79	14 50 51.24	20 56 32.4	0.2186	C+	
ABELL 1990-2	4-09-81	14 51 41.03	28 14 25.7	0.2430	C+	
ABELL 1997-2	5-26-79	14 53 42.45	20 17 48.0	0.2490	C	
ABELL 1997-3	5-26-79	14 53 39.35	20 18 40.3	0.2511	B-	
ABELL 2001-1	5-26-79	14 54 48.75	22 57 13.0	0.1748	B	1
ABELL 2001-2	5-26-79	14 54 45.60	22 57 04.6	0.2084	C	
ABELL 2001-3	5-26-79	14 54 33.06	22 53 48.6	0.1133	B-	S 2
ABELL 2001-4	6-23-79	14 54 45.95	22 56 08.7	0.1743	B-	
ABELL 2003-1	5-11-80	14 56 37.27	19 38 25.5	0.0439	A-	
ABELL 2003-2	4-09-81	14 56 30.86	19 41 13.3	0.2172	C+	3
ABELL 2004-1	4-16-80	14 56 14.64	25 10 13.7	0.0640	A	4
ABELL 2004-2	4-16-80	14 56 18.57	25 10 43.8	0.1366	B	
ABELL 2006-1	4-16-80	14 57 14.81	19 55 21.2	0.1154	A-	S 5
ABELL 2006-2	6-13-80	14 57 22.56	19 54 45.3	0.1174	B	S
ABELL 2008-1	6-05-78	14 57 42.04	23 19 30.5	0.1806	B	6
ABELL 2008-2	6-06-78	14 57 45.08	23 19 46.4	0.1827	B-	
ABELL 2009-1	5-27-79	14 58 05.34	21 34 46.3	0.1573	B	
ABELL 2009-2	5-27-79	14 58 04.30	21 34 00.1	0.1532	B	
ABELL 2009-3	5-27-79	14 58 00.56	21 35 57.5	0.1488	B	
ABELL 2009-4	6-22-79	14 57 59.14	21 36 50.8	0.1520	B	
ABELL 2009-5	6-23-79	14 58 06.58	21 32 51.7	0.1539	C+	
ABELL 2012-1	6-11-80	14 59 37.41	16 43 43.8	0.1520	A	
ABELL 2012-2	2-02-82	14 59 23.11	16 44 58.3	0.1516	A-	7
ABELL 2012-3	2-02-82	14 59 28.53	16 45 32.1	0.1497	A-	8
ABELL 2021-1	6-14-80	15 01 53.15	22 58 39.3	0.0994	C	
GROUP 1-1	4-16-80	14 59 07.26	22 15 17.8	0.1630	B	
GROUP 2-1	4-15-80	14 57 25.18	22 01 34.2	0.1522	A-	
GROUP 2-2	4-15-80	14 57 26.78	22 00 51.4	0.1542	B	9
GROUP 4-1	4-15-80	14 54 01.55	23 48 54.9	0.1676	B-	
GROUP 4-2	4-15-80	14 53 26.17	23 47 39.1	0.0707	A	10
GROUP 4-3	4-15-80	14 53 09.83	23 48 14.3	0.1158	B-	S
GROUP 4-4	4-16-80	14 53 00.15	23 49 44.0	0.0803	C-	

TABLE 1—*Continued*

CLUSTER	DATE	α(1950)	δ(1950)	z	Q	Notes
GROUP 7-1	4-15-80	14 52 26.99	22 57 28.0	0.1037	B+	
GROUP 7-2	4-15-80	14 52 11.40	23 03 01.3	0.0792	B	
GROUP 8-1	4-15-80	14 51 48.58	23 33 42.5	0.1180	A-	S
GROUP 15-1	4-15-80	14 44 09.07	21 54 42.2	0.1121	A-	S
GROUP 15-2	4-15-80	14 44 09.11	21 54 12.6	0.1131	A-	S
GROUP 16-1	4-16-80	14 40 03.44	22 30 54.8	0.0963	B	
GROUP 17-1	4-16-80	14 58 42.76	19 34 08.9	0.1144	B	S
GROUP 17-2	4-16-80	14 58 26.15	19 36 27.8	0.1150	A-	S
GROUP 18-1	6-13-80	15 01 09.03	19 21 48.1	0.1531	B+	
GROUP 19-1	5-11-80	14 56 25.71	19 15 13.3	0.1161	A-	S 11
GROUP 19-2	5-11-80	14 57 38.10	19 15 28.3	0.1404	B-	
GROUP 20-1	6-11-80	14 56 51.36	18 50 38.6	0.1156	A	S
GROUP 21-1	5-11-80	14 52 07.34	19 22 33.1	0.1168	B	S
GROUP 22-1	6-11-80	14 50 13.95	19 26 03.5	0.1157	B+	S
GROUP 23-1	6-11-80	14 46 56.44	18 30 07.5	0.1162	B	S
GROUP 24-1	6-13-80	14 44 03.56	21 29 30.8	0.1040	B	
GROUP 25-1	5-11-80	14 42 07.31	22 36 10.4	0.0990	B	
GROUP 26-1	6-11-80	14 41 44.18	25 29 13.4	0.1180	A-	S
GROUP 30-1	2-06-81	14 48 12.26	27 40 41.2	0.1238	B-	
GROUP 31-1	2-06-81	14 49 09.39	26 23 49.1	0.1849	B+	
GROUP 32-1	6-18-80	14 47 30.12	26 25 35.4	0.1163	A	S 12
GROUP 33-1	2-06-81	14 56 30.01	28 03 00.5	0.1263	B	13
GROUP 34-1	1-09-81	14 55 39.06	23 04 18.8	0.1088	A-	S 14
GROUP 35-1	4-06-81	15 00 13.17	26 03 20.9	0.1428	B+	
GROUP 36-1	4-06-81	14 56 42.63	25 49 36.9	0.1152	B+	S
GROUP 37-1	4-09-81	14 49 30.42	24 42 06.2	0.1191	A-	S
GROUP 38-1	4-06-81	14 52 38.56	18 01 24.8	0.1120	B	S
GROUP 39-1	4-06-81	14 50 32.82	18 26 00.8	0.1179	B	S

SUPERCLUSTER 1615+43 GALAXIES

CLUSTER	DATE	α(1950)	δ(1950)	z	Q	Notes
ABELL 2158-1	6-05-78	16 06 29.45	43 07 19.9	0.1375	A-	S
ABELL 2158-2	6-05-78	16 06 13.72	43 02 46.3	0.0776	B+	15
ABELL 2158-3	6-05-78	16 06 07.03	43 11 03.4	0.1368	B+	S
ABELL 2158-4	6-05-78	16 06 19.21	43 09 18.8	0.0850	A-	
ABELL 2158-5	6-22-79	16 06 57.10	43 06 17.3	0.1837	B-	
ABELL 2158-6	10-24-79	16 06 29.14	43 07 00.8	0.1296	C	S
ABELL 2172-1	6-03-78	16 14 59.15	42 34 15.3	0.1348	B	S
ABELL 2172-2	6-03-78	16 14 49.62	42 31 39.3	0.1399	B-	S
ABELL 2172-3	6-03-78	16 14 32.45	42 31 24.6	0.0232	A	16
ABELL 2172-4	6-04-78	16 14 54.78	42 33 17.3	0.1405	A	S

TABLE 1—*Continued*

CLUSTER	DATE	α(1950)	δ(1950)	z	Q	Notes
ABELL 2179-1	6-21-79	16 18 28.56	42 27 34.7	0.1352	A	S
ABELL 2179-2	6-21-79	16 19 00.91	42 28 59.9	0.1373	B	S
ABELL 2179-3	6-23-79	16 18 28.33	42 28 17.1	0.1341	B	S
ABELL 2183-1	6-04-78	16 19 49.31	42 52 42.7	0.1377	A	S
ABELL 2183-2	6-04-78	16 19 58.69	42 52 53.2	0.1328	A	S
ABELL 2183-3	6-04-78	16 20 11.70	42 53 47.0	0.0593	B	17
ABELL 2183-4	10-24-79	16 19 53.51	42 52 26.9	0.1394	B-	S
ABELL 2187-1	6-06-78	16 22 33.68	41 21 26.4	0.1830	A-	
ABELL 2187-2	6-06-78	16 22 32.26	41 21 47.7	0.1807	B	
ABELL 2187-3	6-23-79	16 22 30.53	41 23 23.2	0.1873	B-	
ABELL 2192-1	6-06-78	16 25 05.26	42 46 52.4	0.1870	B	
ABELL 2192-2	6-21-79	16 24 50.95	42 46 54.8	0.1875	B	
ABELL 2192-3	6-22-79	16 24 58.83	42 48 29.8	0.1839	C	
ABELL 2196-1	6-21-79	16 25 47.39	41 37 02.2	0.1336	B	S
ABELL 2196-2	6-21-79	16 25 51.66	41 36 32.5	0.1288	A	S 18
ABELL 2196-3	6-21-79	16 25 55.32	41 35 21.1	0.1373	C	S
ABELL 2198-1	6-14-80	16 27 28.13	43 57 49.6	0.0800	B	
ABELL 2198-2	6-14-80	16 27 27.36	43 56 53.7	0.1696	B+	
ABELL 2198-3	6-14-80	16 27 28.58	43 54 28.4	0.0796	B-	
ABELL 2211-1	6-11-80	16 32 23.44	41 02 05.9	0.1353	A	S
ABELL 2211-2	6-11-80	16 31 58.59	41 02 45.0	0.1347	B+	S
ABELL 2211-3	10-08-80	16 32 32.31	41 02 44.7	0.1383	C+	S
ABELL 2213-1	4-08-81	16 34 55.17	41 22 00.0	0.1597	B	
GROUP 1-1	10-08-80	16 28 46.97	42 37 47.9	0.0998	C	
GROUP 2-1	6-14-80	16 28 19.94	43 21 23.0	0.1236	B	
GROUP 5-1	6-14-80	16 21 34.69	44 11 36.4	0.1328	B	S
GROUP 6-1	6-11-80	16 20 56.12	42 03 47.8	0.1373	A-	S
GROUP 7-2	6-13-80	16 13 18.58	42 20 50.3	0.1383	B-	S 19
GROUP 8-1	10-08-80	16 10 37.09	44 00 08.8	0.1412	B	S 20
GROUP 11-1	6-14-80	16 29 12.84	41 23 33.0	0.0930	B+	
GROUP 12-1	6-11-80	16 20 45.28	40 40 44.0	0.1330	B+	S
GROUP 13-1	6-14-80	16 06 50.56	42 29 28.9	0.1219	C	
GROUP 15-1	4-08-81	16 10 37.91	42 24 54.7	0.0436	C	21
GROUP 15-2	4-08-81	16 10 42.37	42 24 17.0	0.0375	C	
GROUP 16-1	7-18-80	16 00 21.16	44 47 12.5	0.1328	B+	S 22
GROUP 17-1	10-07-80	15 56 56.15	44 51 53.5	0.1315	B-	S
GROUP 17-2	10-07-80	15 56 54.56	44 51 51.0	0.1378	B-	S
GROUP 18-1	10-06-80	16 07 42.63	46 01 49.5	0.1537	A-	
GROUP 19-1	4-08-81	16 16 26.83	43 16 22.2	0.1318	B+	S

NOTES TO TABLE 1

1. Abell 2001-1.—This galaxy has also been observed by Mason *et al.* (1981). Their redshift is 0.175.
2. Abell 2001-3.—This galaxy has also been observed by Mason *et al.* (1981). Their redshift is 0.111.
3. Abell 2003-2.—This galaxy is a binary. We observed the southeast component.
4. Abell 2004-1.—This is a strong emission line elliptical galaxy. With a 16 minute integration we were able to see the following lines: [O II] λ3727, [Ne III] λ3869, Hγ, [O III] λ4363, Hβ, and [O III] $\lambda\lambda$4959 and 5007.
5. Abell 2006-1.—This is a cD galaxy. We observed the northeast component.
6. Abell 2008-1.—Another cD galaxy. We observed the northeast component.
7. Abell 2012-2.—This galaxy was observed for us with an ITS spectrograph on the Mount Lemmon 1.5 m telescope by Mr. Allen Shafter.
8. Abell 2012-3.—This galaxy was also observed with the Mount Lemmon ITS by Mr. Allen Shafter.
9. 1451+22 Group 2-2.—This is a 6″–8″ binary galaxy. The fainter component was observed.
10. 1451+22 Group 4-2.—This is an emission-line spiral galaxy. [O III] $\lambda\lambda$4959 and 5007 are visible.
11. 1451+22 Group 19-1.—The galaxy is a close double (~8″ separation). We measured the eastern component.
12. 1451+22 Group 32-1. The galaxy was observed for us by Dr. Steven Grandi.
13. 1451+22 Group 33-1.—Another binary galaxy. We observed the southeast component.
14. 1451+22 Group 34-1.—This galaxy was observed with the ITS spectrograph on the Mount Lemmon 1.5 m telescope.
15. Abell 2158-2.—This galaxy is a double. We measured the westernmost component.
16. Abell 2172-3.—This is an emission-line spiral. [O III] $\lambda\lambda$4959, 5007 and Hβ are visible.
17. Abell 2183-3.—Another foreground spiral galaxy.
18. Abell 2196-2.—This galaxy is bluer than a normal elliptical for its redshift.
19. 1615+43 Group 7-2.—The galaxy is a close double. We observed the northeast component.
20. 1615+43 Group 8-1.—This galaxy appears to be a very tight binary. Light from both components entered our slit.
21. 1615+43 Group 15-1.—This is an interesting object. On the POSS "O" plate it appears to be stellar, and on the "E" plate it is slightly nebulous. It appeared extremely fuzzy to us on the TV screen.
22. 1615+43 Group 16-1.—This galaxy was observed for us by Dr. Bruce Margon.

The right ascension and declination of the galaxies are presented in the third and fourth columns of Table 1. These positions were determined by measuring the galaxies and SAO reference stars on the Palomar Sky Survey glass copies with the Kitt Peak two-screw Grant comparator. The x-y measurements were then reduced to right ascension and declination using Don Wells's "ASTRO" program. The standard deviations of the measurements are typically 1″.

The last column in Table 1 contains notes for the galaxies. The letter "S" in this column signifies the galaxy is a supercluster member. Finding charts for the galaxies are presented in Figures 2 and 3 (Plates 5–12).

III. CLUSTER PROPERTIES

The positions, characteristics, and mean redshifts of supercluster member clusters are presented in Table 2. The nonmember clusters' properties appear in Table 3. Clusters which break up into a superposition of two or more redshift systems have multiple entries which are designated by A, B, C, etc. The tables present the following information: First column—The cluster or group number. Second column—The right ascension of the cluster center. Third column—The declination of the cluster center. For the Abell clusters, the cluster center coordinates are those given by Abell (1958). Fourth column—The richness class of the cluster. For the Abell clusters, this was taken from Abell (1958). The richnesses for the poor clusters and groups were derived from galaxy counts made from high quality enlargements of the Palomar Sky Survey glass copies, following Abell's scheme as extended by Bahcall (1980). This classification scheme is summarized in Table 4. Fifth column—The Bautz-Morgan class of the cluster (Bautz and Morgan 1970). For the rich Abell clusters, this was taken from Leir and van den Bergh (1977). The BM types for the poor clusters were estimated from their appearance on the POSS "E" plates. Sixth column—The Rood-Sastry morphological class of the cluster (Rood and Sastry 1971). These were estimated from appearances on the Palomar Sky Survey "E" glass copies. Only clusters with richness -1 or greater were classified. Seventh column—The number of redshifts measured in the cluster. Eighth column—The mean redshift of the cluster. These were calculated by estimating galaxy magnitudes off the Palomar "E" prints and forming a luminosity weighted redshift mean for each cluster. For the rich, condensed clusters, where some virialization has almost certainly taken place, this method best approximates the true cluster redshifts.

A number of the clusters have only one galaxy with a measured redshift. Most of these clusters are either (*i*) Bautz-Morgan type I clusters, wherein the redshift of the central cD galaxy is expected to be very near that of the cluster mean (Quintana and Lawrie 1982), (*ii*) poor clusters dominated by one bright galaxy, which defines the cluster, or (*iii*) clusters which are clearly supercluster nonmembers, for which we made no attempt to improve the cluster redshift.

IV. SUPERCLUSTER PROPERTIES

Figure 4 displays the positions of our supercluster members as projected on the sky. The sizes of these systems are enormous. Even at redshifts greater than 0.1, the superclusters extend across 8° of the sky, implying transverse sizes in excess of $50h^{-1}$ Mpc. Both superclusters appear rather irregular in shape and are somewhat elongated; 1615+43 in particular is reminiscent of the linear morphology associated with the Perseus chain. In addition, both superclusters seem to exhibit core-halo structure, with the rich Abell clusters

TABLE 2

PROPERTIES OF SUPERCLUSTER MEMBERS

MEMBER CLUSTERS IN 1451+22

CLUSTER	α(1950)	δ(1950)	R	BM TYPE	RS TYPE	No. Obs.	<z>
ABELL 1972	14 46.1	24 09	0	I	cD	1	0.1189
ABELL 1976	14 48.1	21 10	1	III	C	3	0.1169
ABELL 1980	14 49.3	22 52	1	II-III	C	3	0.1152
ABELL 1986	14 50.9	22 07	1	III	L	3	0.1182
ABELL 1988A	14 51.2	21 00	0	I	cD	3	0.1160
ABELL 2001A	14 54.8	22 58	1	II:	L	1	0.1133
ABELL 2006	14 57.3	19 52	1	I-II	I	2	0.1164
ABELL 2036	15 09.2	18 15	0	II-III	F	*	0.1163
GROUP 4A	14 53.2	23 48		III	B	1	0.1158
GROUP 8	14 51.8	23 34	-1	I-II	cD	1	0.1180
GROUP 15	14 44.2	21 54	-1	II	B_b	2	0.1126
GROUP 17	14 58.6	19 35	-2	III		2	0.1146
GROUP 19A	14 56.4	19 15	-1	I-II	cD_p	1	0.1161
GROUP 20	14 56.9	18 51	-1	I	cD_p	1	0.1156
GROUP 21	14 52.1	19 23	0	II	C	1	0.1168
GROUP 22	14 50.2	19 26	-1	II-III	F	1	0.1157
GROUP 23	14 46.9	18 30	-2	III		1	0.1162
GROUP 26	14 41.7	25 29	-1	I-II	B	1	0.1180
GROUP 32	14 47.5	26 26	-1	III	C	1	0.1163
GROUP 36	14 56.7	25 50	-2	II-III		1	0.1152
GROUP 37	14 49.5	24 42	-1	I:	cD	1	0.1191
GROUP 38	14 52.7	18 01	-3	II		1	0.1120
GROUP 39	14 50.5	18 26	-1	II	F	1	0.1179

MEMBER CLUSTERS IN 1615+43

CLUSTER	α(1950)	δ(1950)	R	BM TYPE	RS TYPE	No. Obs.	<z>
ABELL 2158B	16 06.6	43 09	0	II-III:	C	3	0.1349
ABELL 2172	16 15.1	42 32	1	II-III	F	3	0.1387
ABELL 2179	16 18.6	42 32	1	III	C	3	0.1360
ABELL 2183	16 19.9	42 50	1	II	C	3	0.1365
ABELL 2196	16 25.7	41 36	0	II-III	F	3	0.1332
ABELL 2211	16 32.4	41 03	1	II-III:	I	3	0.1355
GROUP 5	16 21.6	44 12	-1	I-II	cD	1	0.1328
GROUP 6	16 20.9	42 04	-1	I-II	cD	1	0.1373
GROUP 7	16 13.3	42 21	-2	I		1	0.1383
GROUP 8	16 10.6	44 01	-1	II-III	B	1	0.1412
GROUP 12	16 20.8	40 41	-2	II		1	0.1330
GROUP 16	16 00.4	44 47	-1	I	cD	1	0.1328
GROUP 17	15 56.9	44 52	-2	I		2	0.1339
GROUP 19	16 16.4	43 16	-1	III	I	1	0.1318

* Redshift measured by Schneider, Gunn, and Thuan.

concentrated toward the supercluster centers and along their major axes.

Despite their tremendous sizes, the observed velocity dispersions in the two superclusters are small, $\sigma \approx 500$ km s^{-1} for 1451+22 and $\sigma \approx 750$ km s^{-1} for 1615+43 (cf. Fig. 5). These dispersions are slightly larger than the true dispersions because of measuring errors and errors in the mean cluster velocities caused by the motion of galaxies within the clusters. We modeled this motion by dividing our clusters and groups into three classes. For clusters with an Abell richness 0 or greater, our data give 650 km s^{-1} as the average standard deviation for the line-of-sight motion of bright galaxies near the cluster centers. For poor clusters we adopted 200 km s^{-1} as the mean internal velocity dispersion. This value is typical of the dispersions found by Gott and Turner (1977) in 23 small groups which show no evidence of background contamination. In addition, we chose 200 km s^{-1} as an estimate of the velocity error in Bautz-Morgan type I clusters, since the central cD galaxy almost certainly lies near the dynamical center of the cluster (Quintana and Lawrie 1982). When these values for the internal cluster velocity dispersions are used in an analysis of variance calculation, the true supercluster velocity dispersions become $\sigma_{true} \approx 450$ km s^{-1} for 1451+22 and $\sigma_{true} \approx 700$ km s^{-1} for 1615+43. These values are insensitive to the precise model of the cluster velocity dispersions.

The morphological and dynamical properties described above are confirmed for 1451+22 by the

TABLE 3

PROPERTIES OF NONMEMBER CLUSTERS

NON MEMBER CLUSTERS IN THE FIELD OF 1451+22

CLUSTER	α(1950)	δ(1950)	R	BM TYPE	RS TYPE	No. Obs.	<z>
ABELL 1960	14 42.2	19 33	1	II-III	F	1	0.1876
ABELL 1984	14 50.2	28 09	2	II	L	1	0.1242
ABELL 1988B	14 51.2	21 00		III		1	0.2186
ABELL 1990	14 51.6	28 17	3	III	F	1	0.2430
ABELL 1997	14 53.6	20 17	0	III	F	2	0.2499
ABELL 2001B	14 54.8	22 58	1	II:	L	2	0.1746
ABELL 2003	14 56.4	19 39	1	II-III:	F	1	0.2172
ABELL 2004A	14 56.4	25 08	0	II	C	1	0.0640
ABELL 2004B	14 56.4	25 08		III		1	0.1366
ABELL 2008	14 57.8	23 20	2	II	C	2	0.1810
ABELL 2009	14 58.0	21 34	1	I-II:	L	5	0.1530
ABELL 2012	14 59.5	16 43	1	III	L	3	0.1511
ABELL 2021	15 01.3	23 13	1	III	I	1	0.0994
GROUP 1	14 59.1	22 15	-1	III	C	1	0.1630
GROUP 2	14 57.4	22 01	-1	III	B_b	2	0.1532
GROUP 4B	14 54.0	23 49	-1	III	F	1	0.1676
GROUP 7	14 52.4	23 58	-1	II	C	1	0.1037
GROUP 16	14 40.2	22 31	-2	II		1	0.0963
GROUP 18	15 01.3	19 22	0	II-III	B	1	0.1531
GROUP 19B	14 57.6	19 15	0	I	cD	1	0.1404
GROUP 24	14 44.1	21 30	0	II	C	1	0.1040
GROUP 25	14 42.1	22 36	-1	II-III	F	1	0.0990
GROUP 30	14 50.2	27 41	-2	II-III:		1	0.1238
GROUP 31	14 49.2	26 24	-1	II-III:	I	1	0.1849
GROUP 33	14 56.5	28 03	-2	II		1	0.1263
GROUP 34	14 55.7	23 04	-3	II		1	0.1088
GROUP 35	15 00.2	26 04	-1	I-II:	C	1	0.1428

NON MEMBER CLUSTERS IN THE FIELD OF 1615+43

CLUSTER	α(1950)	δ(1950)	R	BM TYPE	RS TYPE	No. Obs.	<z>
ABELL 2158A	16 06.6	43 09		III	I	2	0.0797
ABELL 2158C	16 06.6	43 09		III		1	0.1837
ABELL 2187	16 22.6	41 23	0	I-II	L	3	0.1829
ABELL 2192	16 25.0	42 47	1	II-III:	F	3	0.1868
ABELL 2198A	16 26.5	43 56	2	III:	F	2	0.0798
ABELL 2198B	16 26.5	43 56		III	C	1	0.1696
ABELL 2213	16 34.9	41 23	1	III	I	1	0.1597
GROUP 1	16 28.8	42 38	0	II:	C	1	0.0998
GROUP 2	16 28.3	43 21	-1	II	I	1	0.1236
GROUP 11	16 29.2	41 24	0	III	F	1	0.0930
GROUP 13	16 06.8	42 29	-1	I-II:	cD_p	1	0.1219
GROUP 15	16 10.7	42 25	-2	III		2	0.0412
GROUP 18	16 07.7	46 02	-3	III		1	0.1537

recent redshift measurement of Abell 2036 by Schneider, Gunn, and Hoessel (1983). Although this richness class 0 cluster lies almost 6°, or $30h^{-1}$ Mpc, southeast of the supercluster's center, its redshift ($z = 0.1163$) is, within measurement error, identical to the mean supercluster redshift. The inclusion of this cluster increases the size and volume of the supercluster while elongating it along the major axis inferred from the other Abell clusters. The already small velocity dispersion for this system, however, is lowered still further.

Figure 6 contains perspective plots of all the observed clusters. The high density contrast in redshift space which the superclusters exhibit over their immediate surroundings is obvious. Figures 5 and 6 show that there are no cases of ambiguous membership in either system. The nearest nonmember of 1451+22 has a redshift 3.9 standard deviations away from the supercluster mean; in 1615+43, the nearest nonmember stands 4.3 σ away in redshift space. Figure 6 also illustrates superclustering among some of the nonmember clusters. The Abell clusters 2009 and 2012, along with groups 2 and 18, form a supercluster at $z \approx 0.153$, which overlaps the eastern edge of 1451+22. Despite a 5° spread on the sky, these four clusters have an exceedingly small velocity dispersion ($\sigma_v \approx 225$ km s^{-1}). It is very probable that this system extends beyond the

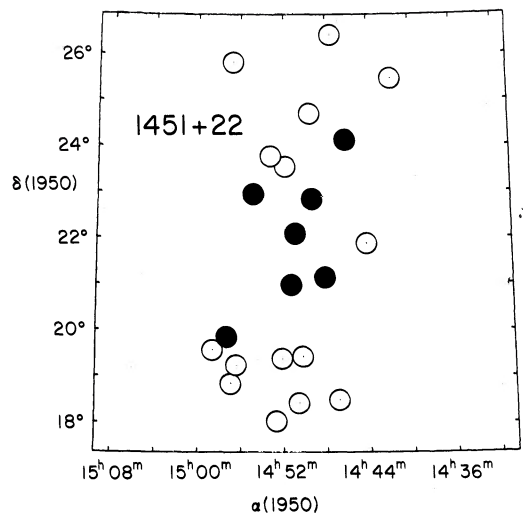

FIG. 4a

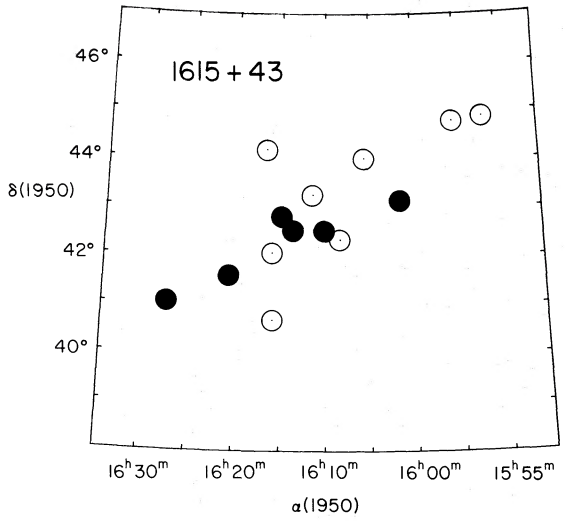

FIG. 4b

FIG. 4.—The locations of the observed supercluster members. Filled circles are Abell clusters shown to Abell's (1958) defining diameters; open circles refer to member groups and poor clusters.

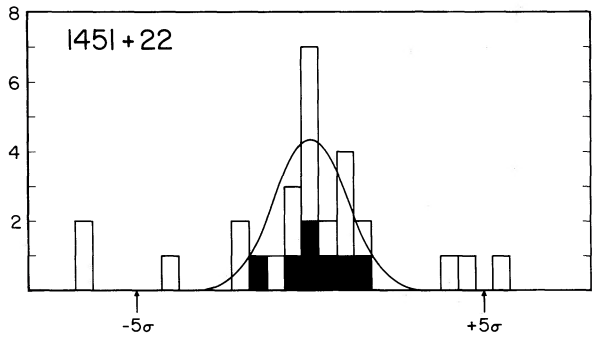

FIG. 5a

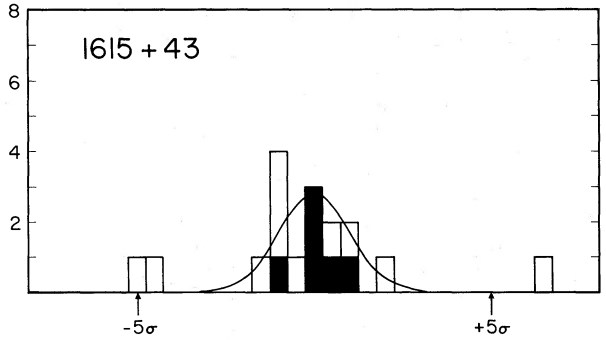

FIG. 5b

FIG. 5.—Distribution of redshifts of observed superclusters members and closest (in redshift) nonmember galaxies. Bins are $\sigma/2$ wide. Filled rectangles represent Abell clusters. Open rectangles include member groups and poor clusters as well as individual nonmember galaxies. Curves are Gaussian fits to weighted data as described in the text. (*a*) 1451+22: $\langle z \rangle = 0.11613$, $\sigma(z) = 0.00188$; and (*b*) 1615+43: $\langle z \rangle = 0.13542$, $\sigma(z) = 0.00274$.

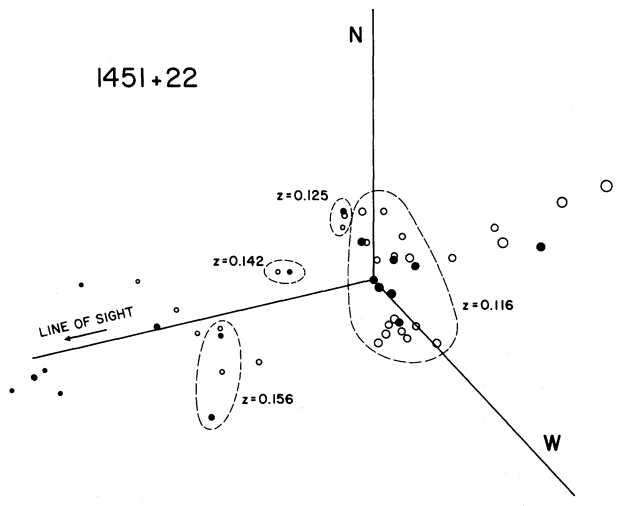

FIG. 6a

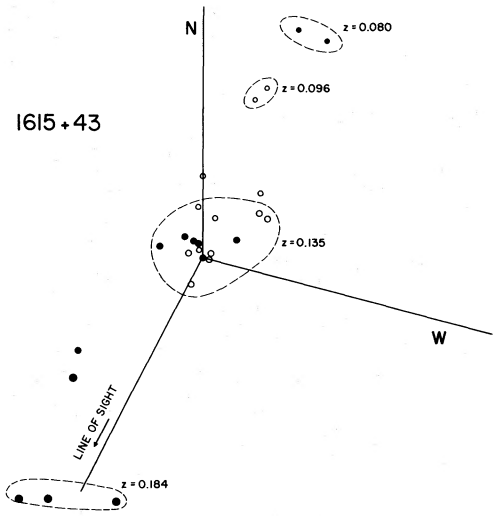

FIG. 6b

FIG. 6.—Perspective plot of the clusters observed in the fields of 1451+22 and 1615+43. The radius of each circle is 1 Mpc. Filled circles are Abell clusters, open circules represent poorer groups. The axes are orthogonal and of equal length in real space.

TABLE 4

CLUSTER RICHNESS CRITERIA

Richness	Counts
3	130–199
2	80–129
1	50–79
0	30–49
−1	20–29
−2	10–19
−3	<10

region of our survey and contains other rich clusters. The same is true at the northern edge of 1451+22, where groups 30 and 33 form an association with Abell 1984 at $z \approx 0.125$. In 1615+43, Abell clusters 2187, 2192, and a component of 2158 form a background supercluster at $z \approx 0.184$, while another component of 2158 and Abell 2198 comprise a foreground system of $z \approx 0.080$. A system at $z \approx 0.096$ is also identifiable in this field.

Although both superclusters span regions over $50h^{-1}$ Mpc, neither exhibits evidence of having an internal velocity gradient. In 1451+22, the strongest correlation of cluster redshift against projected supercluster position occurs at a position angle of $\sim 320°$ and yields a gradient of ~ 50 km s^{-1} degree^{-1}. The correlation is only marginally significant, however, as the two quantities still have a 20% probability of being unrelated. No significant correlation exists in the data for 1615+43. If these superclusters are flattened systems, their major axes must be within $\sim 10°$ of the plane of the sky.

V. GALAXY SELECTION AND DATA BIASING

Previous surveys of the nearest superclusters were performed by measuring magnitude-limited samples of galaxies over well defined regions of the sky. For superclusters at redshifts $z \sim 0.1$, whose brightest galaxies have an $m_v \sim 16$, this is impractical. This procedure would require over 500 redshift measurements and use ~ 250 hr of 3 m telescope time to sample just 1 mag of a supercluster's luminosity function. The Abell clusters, however, are a statistically complete sample of objects which can be used to find and study superclusters (cf. Rood 1976; Thuan 1980). With but one exception (Abell 2017, which we judged to be a nonmember), we measured the redshifts of all 15 Abell clusters which project within 4° of the nominal center of 1451+22. In addition, we measured the redshifts of two Abell clusters which were 6° from the center but close to outlying groups of galaxies which proved to be members (cf. the following discussion). The redshifts of these two clusters, Abell 2012 and Abell 1984, showed that they were not members of the supercluster.

In the supercluster 1615+43 we measured the redshifts of all clusters within 6° of the center that have redshifts estimated by Leir and van den Bergh (1977) of $z < 0.18$. Because these estimated redshifts are accurate to 20%, the survey of 1615+43 included all potential rich cluster members within the 6° radius. The surveys are thus complete for Abell clusters within a 4° radius of 1451+22 and a 6° radius centered on 1615+43. At the redshifts of the superclusters (0.1161 and 0.1354), these radii respectively correspond to $20h^{-1}$ Mpc and $35h^{-1}$ Mpc. These dimensions are comparable to or larger than those of other known superclusters.

A given supercluster, however, contains only a few Abell clusters. In terms of Abell clusters, 1451+22 is now the richest supercluster studied, but it contains only eight rich clusters. Supercluster 1615+43 contains only six rich clusters. To investigate the dynamical and morphological properties of these systems, we need a larger sampling of the spacial and velocity fields. Consequently, we devised a galaxy selection criteria designed to find additional supercluster members.

Sandage (1973*a*) and others have noted the very small dispersion in the intrinsic colors of bright E and SO galaxies [$\sigma_{(B-V)} \approx 0.028$ mag]. The apparent colors of these objects change with redshift, however, as the distinctive spectral continuum redshifts through the *B* and *V* filter bandpasses (Sandage 1973*a*; Butcher *et al.* 1976). We took advantage of this fact and chose to observe galaxies whose "E" magnitude and "E" − "O" color, as estimated from the Palomar prints, were comparable to that of the brightest galaxies in the member rich clusters. We estimate that in the regions within 5° of the nominal supercluster centers, we have identified 90% of the galaxies which satisfy this qualitative criteria.

As Table 1 shows, this technique was extremely successful. Approximately half of the candidates so chosen proved to be supercluster members. These new groups and poor clusters improved the statistical significance of our results and revealed the enormous extent of these systems. This sampling of groups and clusters is a biased one, however. The number of supercluster galaxies has been artificially enhanced over that of the field by the selection criteria. In order to understand the significance of our results, we must estimate the effects of this bias. We do so as follows:

Assume the distribution of absolute magnitudes of first ranked galaxies in all clusters satisfies a Gaussian distribution with dispersion σ_m about some mean. If all the galaxies chosen for measurement have the same apparent magnitude, then the resulting distribution of redshifts can be approximated by a Gaussian with dispersion $\sigma_m/5$ in log *z*. For the reasonable value of $\sigma_m \sim 0.35$ (Sandage 1973*b*; Hoessel, Gunn, and Thuan 1980) at a mean redshift of $z \approx 0.12$, this absolute magnitude dispersion translates into a minimum dispersion in redshift space of $\sigma_{z(m)} \approx 0.020$.

The bias introduced by our color criteria can be approximated from the color-redshift given by Sandage (1973*a*). We optimistically estimate that our qualitative visual color estimates off the Palomar prints have an error of $\sigma_c \geq 0.1$. If we assume the intrinsic color dispersion of first-ranked galaxies is negligible, a color-redshift slope of ~ 4 yields a lower limit to the color selection redshift dispersion $\sigma_{z(c)} \sim 0.025$.

Combining these two limits gives us the theoretical lower limit to the redshift resolution of our sampling criteria of $\sigma_z \approx 0.015$. In practice, we did not achieve this accuracy. The data in Table 1 indicate our redshift resolution was probably closer to $\sigma_z \approx 0.03$. But even the theoretical limit derived above is an order of magnitude larger than the dispersion observed in both superclusters. We therefore conclude that the small velocity dispersions and high redshift space density contrasts are real properties of both superclusters and not an artifact of the selection criteria. The method works well because of the superclusters' high contrast in either physical or redshift space. The candidates are either in the supercluster, or clearly out.

V. DISCUSSION

There are now five rich superclusters with substantial dynamical and morphological data available: Coma/Abell 1367 (Gregory and Thompson 1978), Hercules/Abell 2197 (Chincarini, Rood, and Thompson 1981), Perseus (Gregory, Thompson, and Tifft 1981), and 1451+22 and 1615+43 (this paper). A comparison of these systems is instructive.

All the superclusters studied so far have a characteristic size of $50h^{-1}$ Mpc, a number which agrees with that predicted from the statistical studies of rich cluster surface density (Abell 1961; Hauser and Peebles 1973). The binary supercluster Coma/Abell 1367 is the smallest and poorest, consisting mainly of two rich clusters separated by $21h^{-1}$ Mpc on the sky. 1451+22 is currently the richest supercluster, containing eight Abell clusters scattered over an area spanning $50h^{-1}$ Mpc.

The projected shapes on the sky are all aspherical. Perseus and 1615+43 appear as lines of clusters strung across the sky, surrounded by amorphous halos. 1451+22 is less flattened but still clearly elongated. Although Hercules appears to be more regular, it shows evidence for an internal velocity gradient. These data, along with the shape derived for the local supercluster (Tully 1982), point to the probability that superclusters are flattened disklike systems.

Perhaps the most intriguing supercluster properties are derived from the galaxy redshift distribution in and around each supercluster. To date, all of the systems have small velocity dispersions. Hercules is by far the thickest supercluster known, with an implied 2 σ depth of $50h^{-1}$ Mpc. 1451+22, however, is almost two dimensional, having a 2 σ front-to-back size of only $18h^{-1}$ Mpc. The small dispersions and projected shapes of Perseus and 1615+43 suggest these systems have one dimensional morphologies. Around each supercluster are large ($\sim 50h^{-1}$ Mpc) regions almost devoid of bright galaxies.

The above properties seem consistent with dissipative collapse models for the early universe, such as those proposed by Zel'dovich (1978) and Doroshkevich *et al.* (1974, 1980). In these models, the growth of adiabatic perturbations in the prerecombination epoch precipitates the formation of compressed gas layers, or pancakes. Perturbations with scale lengths of $40h^{-1}$ Mpc create the systems now identified as superclusters, while the longer scale perturbations damp out in the radiation dominated plasma. In the models one dimensional structures, such as Perseus and perhaps 1615+43, form when two of these pancakes intersect.

This scenario provides a natural explanation for the observed sizes and shapes of superclusters. One disconcerting point does arise from the observations, however. Thus far, all of the superclusters studied appear to have their major axes on, or close to, the plane of the sky. Only Hercules, tipped 27° into the sky, has any measurable inclination. The binary Coma system, the 1451+22 complex, and both linear superclusters have no obvious velocity gradients, implying these systems are perpendicular to our line of sight. This set of supercluster orientations seems somewhat unlikely. To compound the problem, 1451+22 and 1615+43 were originally identified through the projected density enhancement of Abell clusters. Because this criterion selects against face-on systems in favor of superclusters with large inclinations, this sample of superclusters orientation angles is even more improbable.

An explanation for the apparent orientations does exist, however. Supercluster geometries have been derived by making the assumption that observed velocity dispersions reflect an unperturbed Hubble flow. This may not be the case. If gravitational interactions among supercluster members are significant, the Hubble flow within rich superclusters may be slowed. This would result in a decrease in the observed velocity dispersions and implied depths, and an increase in the measured redshift space density contrasts. The overall effect would be to flatten the systems against the plane of the sky and lower their apparent inclination angles.

The easiest way to distinguish between these two interpretations is through radial velocity measurements in superclusters. If the Hubble distortion in the plane of a pancake or filamentary supercluster is small, most systems should display a significant velocity gradient. An inclination angle of only 10° would be revealed by an observable velocity difference of 500 km s^{-1} across the system, and inclinations up to $\sim 65°$ would be easily visible in any redshift survey. If gravitational slowing is important, however, superclusters with large implied inclinations should be rare.

Radial velocity measurements of supercluster member galaxies also offer the possibility of measuring the density of matter on the largest possible scale. If the geometry and structure of these systems can be understood, the observed velocity dispersions can be used to measure the effect of internal gravitational interactions upon supercluster dynamics. This in turn can yield the matter density within superclusters and eventually lead to Ω_0.

We wish to thank Drs. S. Grandi and B. Margon and Mr. Allen Shafter for observing several galaxies in this program. We are grateful to Kitt Peak National Observatory and especially Mark Hanna and Glen Pickens for access to their excellent photographic facilities. This work was supported in part by NASA contract NAS 5-24463. NSF declined support for this work.

REFERENCES

Abell, G. O. 1958, *Ap. J. Suppl.*, **3**, 211.
———. 1961, *A.J.*, **66**, 607.
Bahcall, N. A. 1980, *Ap. J.* (*Letters*), **238**, L117.
Bautz, L. P., and Morgan, W. W. 1970, *Ap. J.* (*Letters*), **162**, L149.
Bogart, R. S., and Wagoner, V. 1973, *Ap. J.*, **181**, 609.
Butcher, H., Oemler, A., Tapia, S., and Tarenghi, M. 1976, *Ap. J.* (*Letters*), **209**, L11.
Chincarini, G., Rood, H. J., and Thompson, L. A. 1981, *Ap. J.* (*Letters*), **249**, L47.
de Vaucouleurs, G. 1975*a*, *Ap. J.*, **202**, 319.
———. 1975*b*, *Ap. J.*, **202**, 610.
Doroshkevich, A. G., Kotok, E. V., Novikov, I. D., Polyudov, A. N., Shandarin, S. F., and Sigov, Yu. S. 1980, *M.N.R.A.S.*, **192**, 321.
Doroshkevich, A. G., Sunyaev, Ra. A., and Zel'dovich, Ya. B. 1974, in *IAU Symposium 63, Confrontation of Cosmological Theories with Observational Data*, ed. M. S. Longair (Dordrecht: Reidel), p. 213.
Ford, H. C., Harms, R. J., Ciardullo, R., and Bartko, F. 1981, *Ap. J.* (*Letters*), **245**, L53 (Paper I).
Gott, J. R., and Turner, E. L. 1977, *Ap. J.*, **213**, 309.
Grandi, S. A. 1982, U.C.L.A. Ast. Image Anal. Lab. Tech. Rep. 1 (2nd ed.).
Gregory, S. A., and Thompson, L. A. 1978, *Ap. J.*, **222**, 784.
Gregory, S. A., Thompson, L. A., and Tifft, W. G. 1981, *Ap. J.*, **243**, 411.
Harms, R. J., Ford, H. C., Ciardullo, R., and Bartko, F. 1981, in *The Tenth Texas Symposium on Relativistic Astrophysics*, ed. R. Ramaty and F. C. Jones (New York: New York Academy of Sciences), p. 178 (Paper II).
Hauser, M. G., and Peebles, P. J. E. 1973, *Ap. J.*, **185**, 757.
Hoessel, J. G., Gunn, J. E., and Thuan, T. X. 1980, *Ap. J.*, **241**, 486.
Leir, A. A., and van den Bergh, S. 1977, *Ap. J. Suppl.*, **34**, 381.
Mason, K. O., Spinrad, H., Bowyer, S., Reichert, G., and Stauffer, J. 1981, *A.J.*, **86**, 803.
Miller, J. S., Robinson, L. B., and Schmidt, G. D. 1980, *Pub. A.S.P.*, **92**, 702.
Miller, J. S., Robinson, L. B., and Wampler, E. J. 1976, *Adv. Electronics Electron Phys.*, **40**, 693.
Murray, S. S., Forman, W., Jones, C., and Giacconi, R. 1978, *Ap. J.* (*Letters*), **219**, L89.
Quintana, H., and Lawrie, D. G. 1982, *A.J.*, **87**, 1.
Robinson, S. B., and Wampler, E. J. 1972, *Pub. A.S.P.*, **84**, 161.
Rood, H. J. 1976, *Ap. J.*, **207**, 16.
Rood, H. J., and Sastry, G. N. 1971, *Pub. A.S.P.*, **83**, 313.
Sandage, A. 1973*a*, *Ap. J.*, **183**, 711.
———. 1973*b*, *Ap. J.*, **183**, 731.
Schneider, D. P., Gunn, J. E., and Hoessel, J. G. 1983, *Ap. J.*, **264**, 337.
Stone, R. P. S. 1977, *Ap. J.*, **218**, 767.
Tarenghi, M., Chincarini, G., Rood, H. J., and Thompson, L. A. 1980, *Ap. J.*, **235**, 724.
Tarenghi, M., Tifft, W. G., Chincarini, G., Rood, H. J., and Thompson, L. A. 1979, *Ap. J.*, **234**, 793.
Thuan, T. X. 1980, in *Physical Cosmology, Les Houches Session XXXII*, ed. R. Balian, J. Audouze, and D. Schramm (Amsterdam: North-Holland), p. 277.
Tully, R. B. 1982, *Ap. J.*, **257**, 389.
Zel'dovich, Ya. B. 1978, in *IAU Symposium 79, The Large Scale Structure of the Universe*, ed. M. S. Longair and J. Einasto (Dordrecht: Reidel), p. 409.

FRANK BARTKO: Martin Marietta Corporation, Code 0561, P.O. Box 179, Denver, CO 80201

ROBIN CIARDULLO and HOLLAND FORD: Space Telescope Science Institute, Homewood Campus, Baltimore, MD 21218

RICHARD HARMS: University of California, San Diego, Center for Astrophysics and Space Sciences, C-011, La Jolla, CA 92093

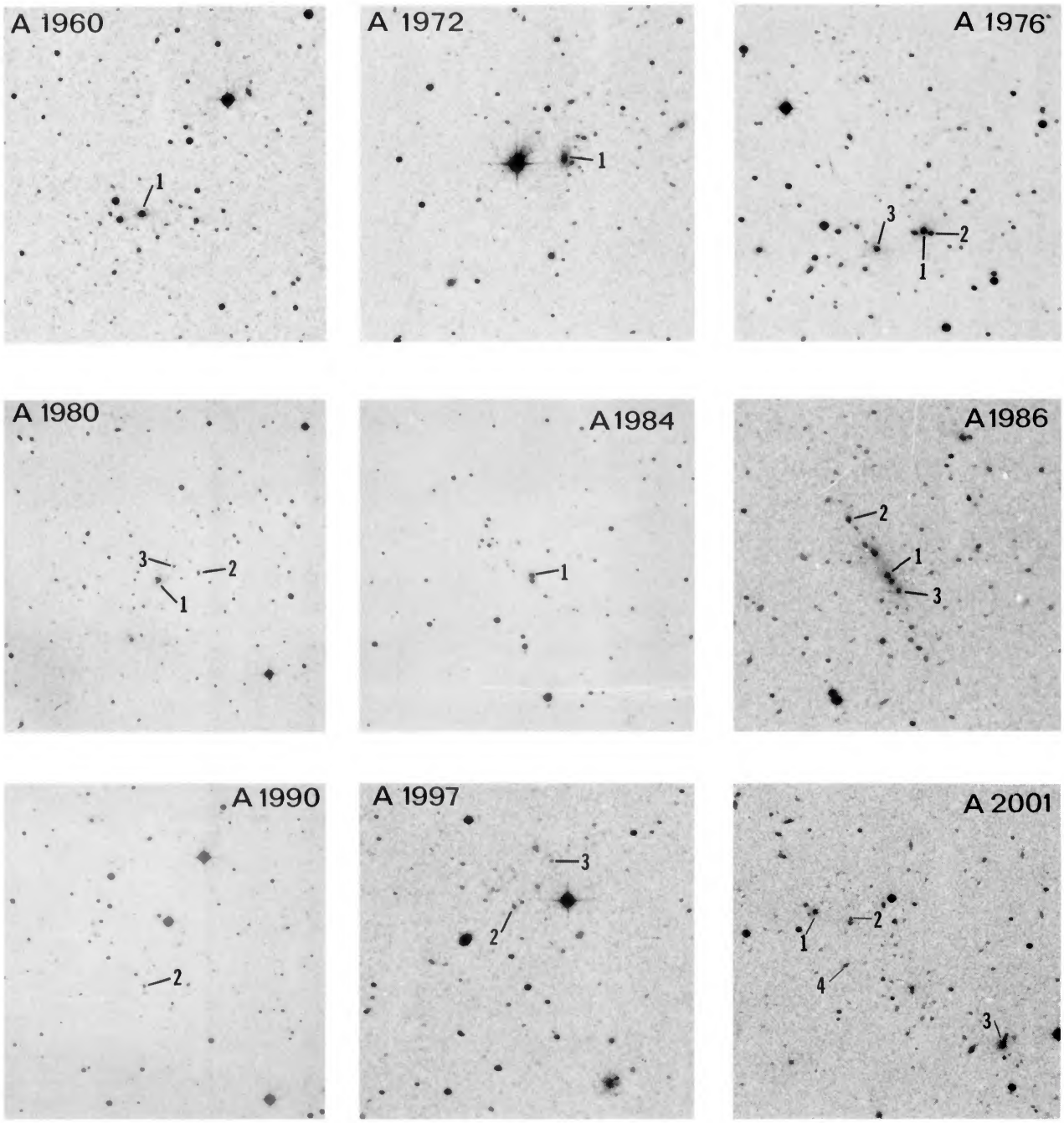

FIG. 2*a*

FIG. 2.—Finding charts for the measured galaxies in the field of 1451+22 reproduced from glass copies of the Palomar Sky Survey "E" plates. Plate scales are as follows: 10.″0 mm^{-1} for Abell 1984 and 1990, 10.″2 mm^{-1} for groups 21, 22, 30, 31, 33, and 35–39, and 7.″5 mm^{-1} for all others.

CIARDULLO *et al.* (*see* page 29)

PLATE 6

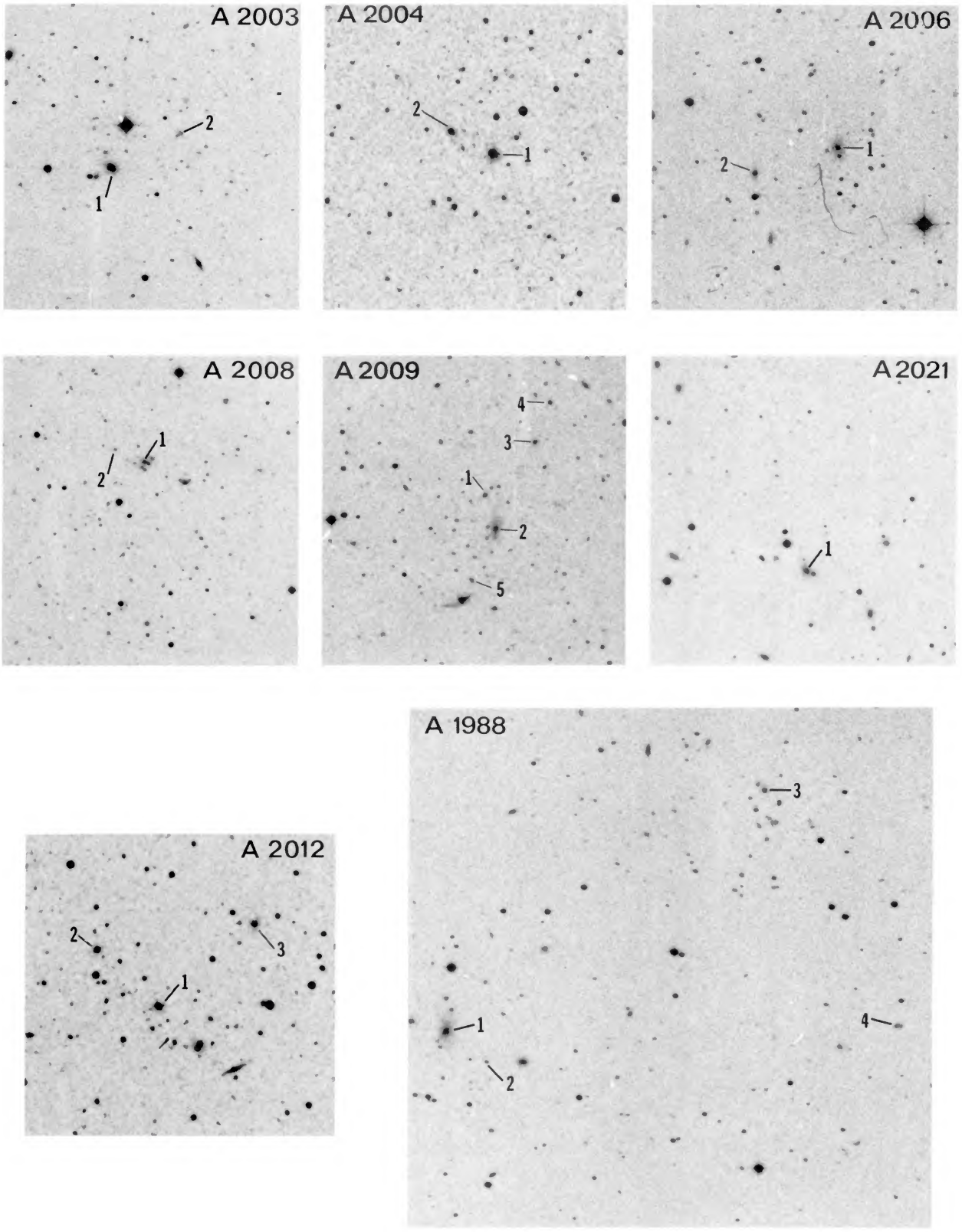

FIG. 2*b*

CIARDULLO *et al.* (*see* page 29)

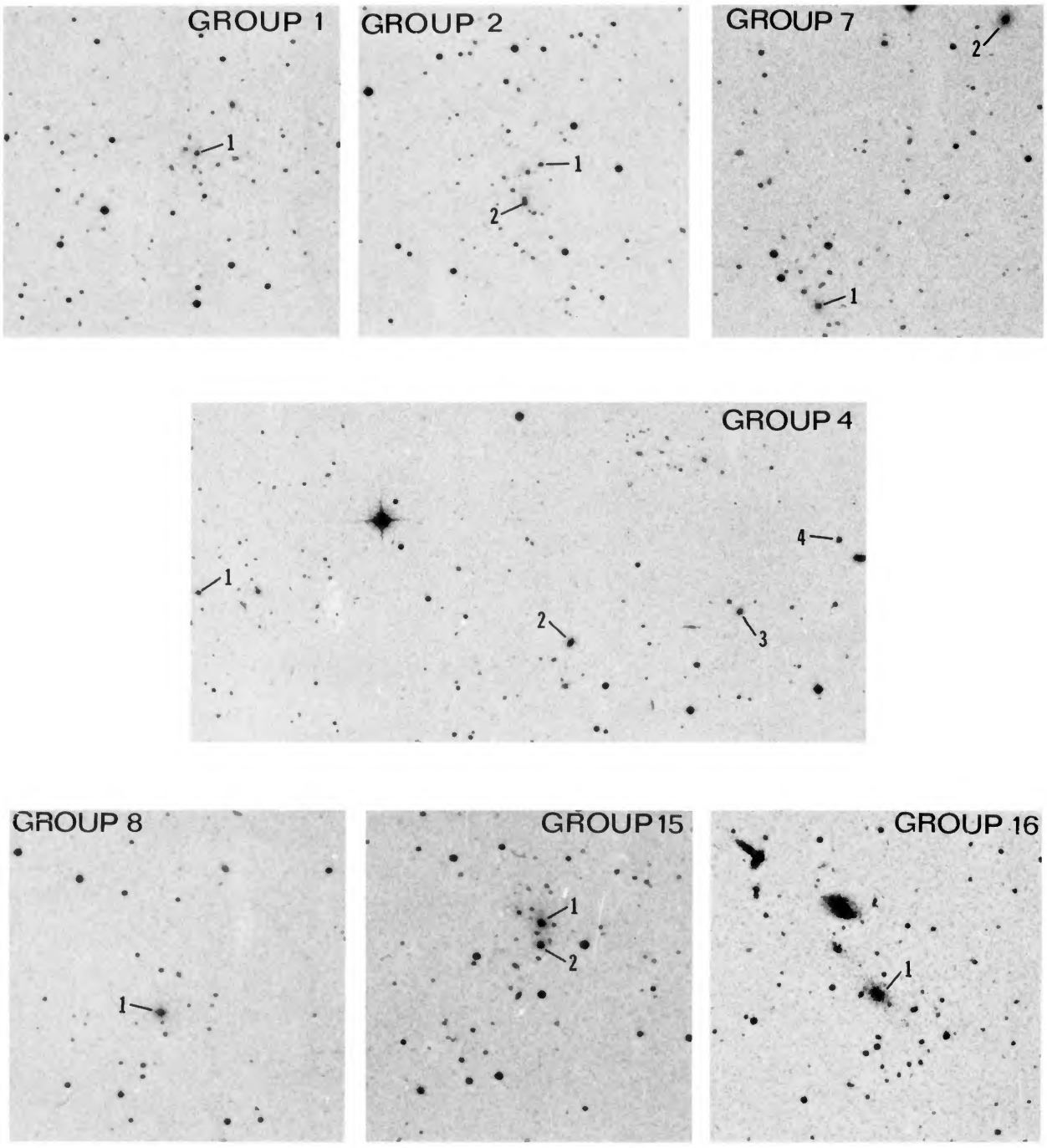

FIG. 2c

CIARDULLO *et al.* (*see* page 29)

PLATE 8

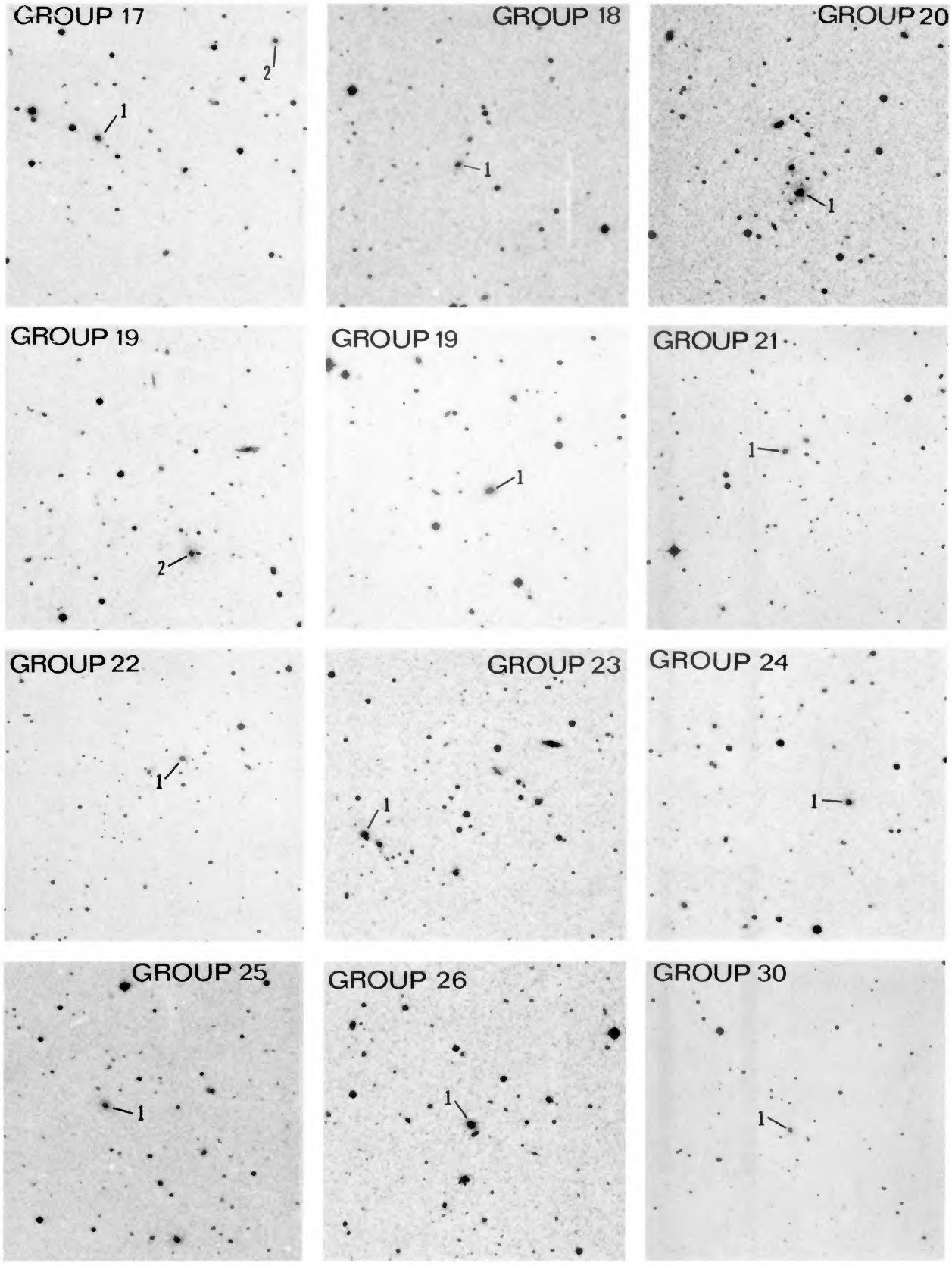

FIG. 2*d*

CIARDULLO *et al.* (*see* page 29)

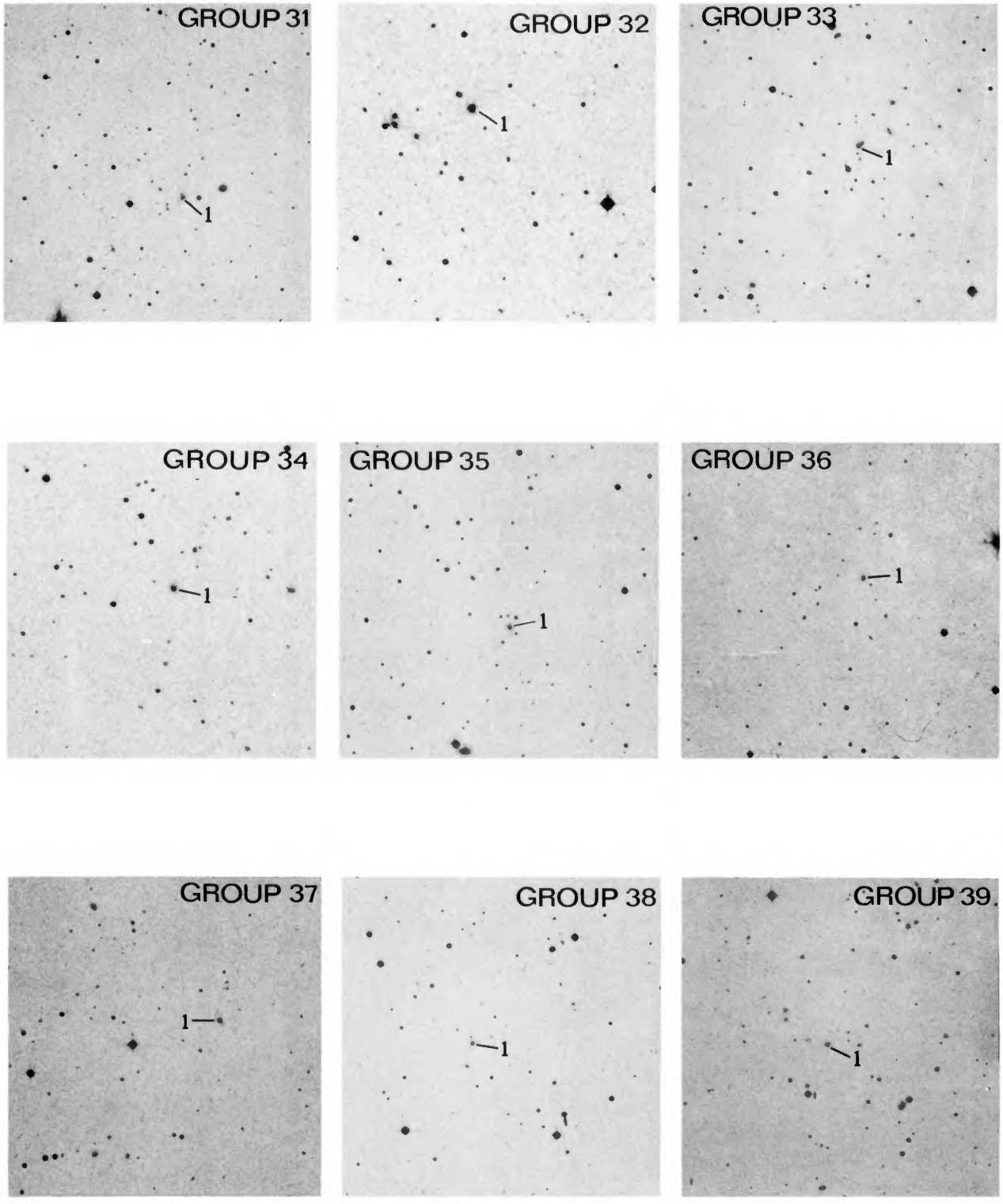

FIG. 2*e*

CIARDULLO *et al.* (*see* page 29)

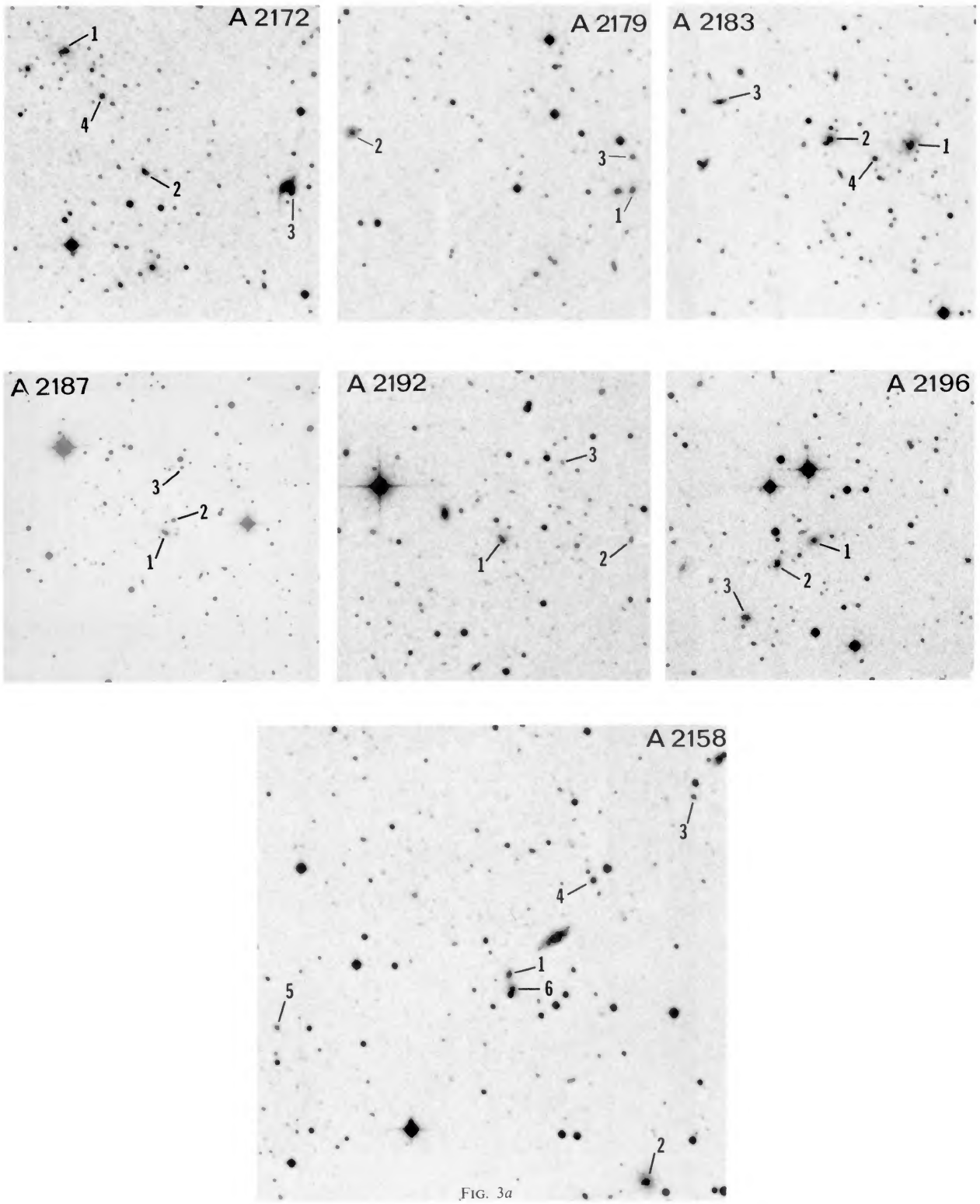

FIG. 3*a*

FIG. 3.—Finding charts for the measured galaxies in the field of 1615+43. Abell 2187 and 2213 and groups 7, 8, and 15–19 have a 10.″2 mm^{-1} plate scale. Plate scale for the remainder is 7.″5 mm^{-1}.

CIARDULLO *et al.* (*see* page 29)

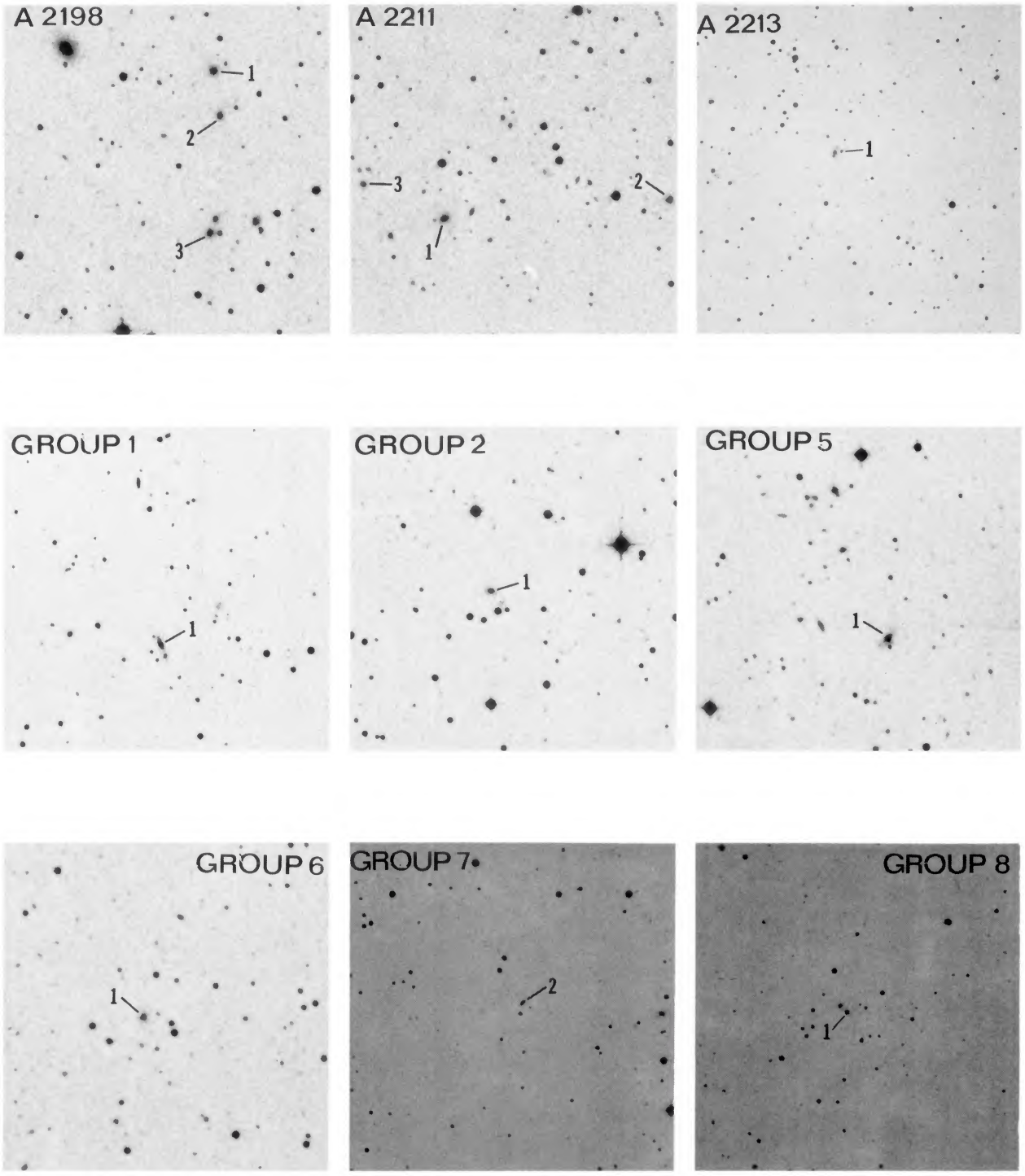

FIG. 3*b*

CIARDULLO *et al.* (*see* page 29)

PLATE 12

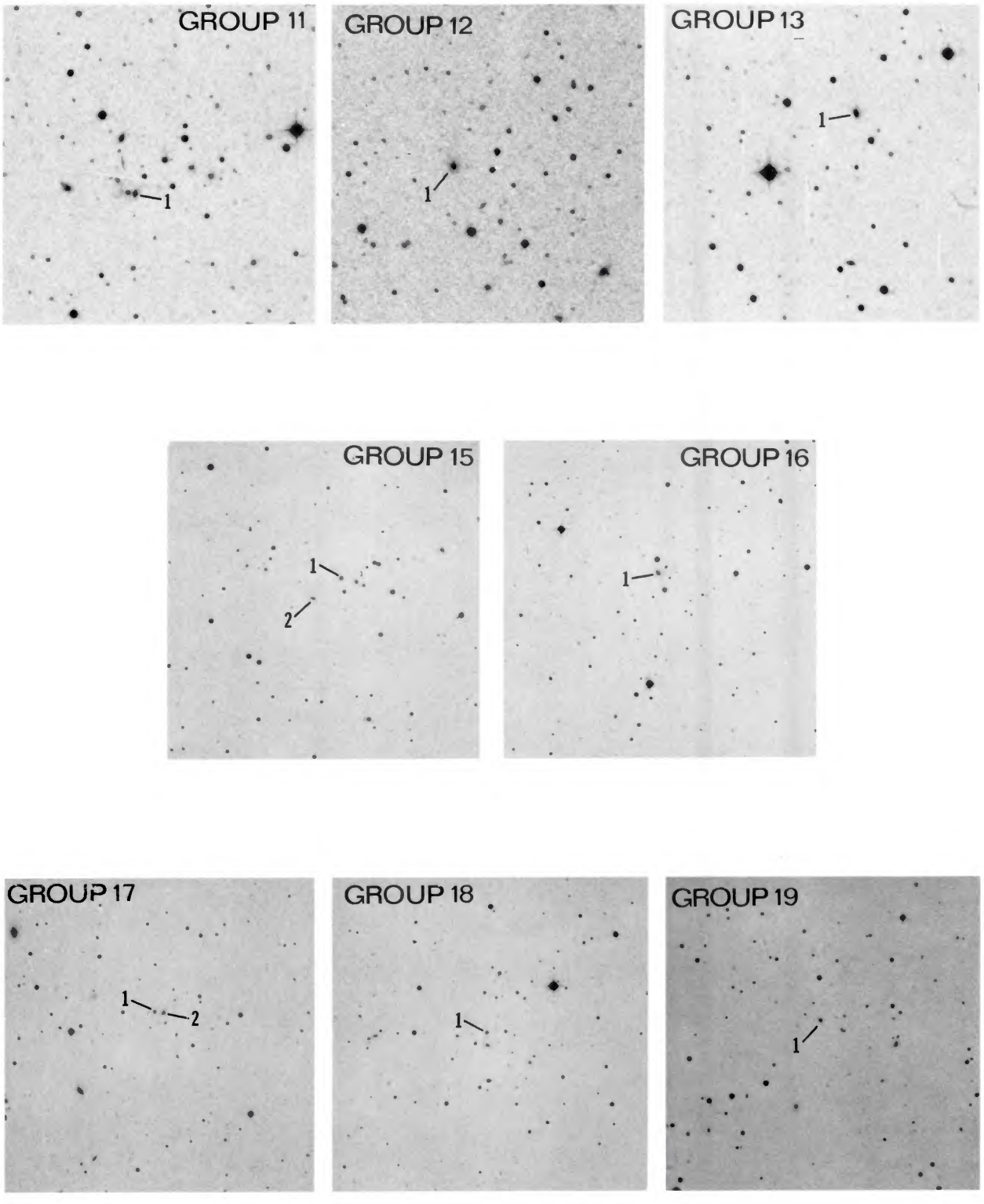

FIG. 3c

CIARDULLO *et al.* (*see* page 29)